RF power experiments in WEST to prepare for next-step fusion device operation

Remi Dumont*, *Theo* Fonghetti, *Julien* Hillairet, *Patrick* Maget, *Pierre* Manas, and the WEST team**

CEA, IRFM, F-13108 Saint-Paul-lez-Durance, France.

Abstract. The WEST superconducting tokamak, featuring a full tungsten environment and equipped with an actively cooled ITER-grade divertor, provides valuable inputs for future ITER operation. One of its distinctive features is that auxiliary plasma heating and current drive is exclusively supplied by radiofrequency (RF) systems. Scenario development supported by integrated modelling has allowed pulses exceeding 1300 s and 2.6 GJ of energy to be performed, based on feedback-controlled plasma current sustained by LHCD power in order to achieve a zero-loop voltage target. In this contribution, we review recent progress and near-term plans related to plasma scenario performance improvement using RF waves in WEST, directly relevant to the operation of future fusion devices in full metal environments.

1 Introduction

WEST is a tokamak equipped with an actively cooled ITER-grade tungsten (W) divertor, as well as a superconducting toroidal magnetic field system producing a magnetic field up to $B_0 \sim 3.7$ T at major radius $R_0 \sim 2.5$ m (typical minor radius $a_0 \sim 0.5$ m). Several plasma configurations (lower/upper X-point, double-null) allow various aspects related to the operation of future magnetic fusion devices to be explored [1]. Among these aspects, developing long pulses, i.e. discharges with durations well above the plasma confinement time and approaching plasma-wall interaction timescales, is of paramount importance [2].

One of the distinctive features of the WEST tokamak is the fact that the auxiliary power for plasma heating and current drive is exclusively supplied by radiofrequency (RF) sources. Its Lower Hybrid Current Drive (LHCD) system consists of two antennas: a fully-active (resp. passive-active) multijunction launcher with a parallel refractive index ($n_\parallel$) spectrum typically centered around $n_\parallel \sim 2$ (resp. 1.7) able to provide up to 4 MW (resp. 3 MW) power and drive the plasma current (up to $I_p \sim 1$ MA) in continuous wave (CW) conditions, at frequency 3.7 GHz. In addition, the Ion Cyclotron Resonance Frequency (ICRF) system, with 3 load-resilient (internal) conjugate-T antennas, is capable of coupling up to 9 MW during 30 s or up to 3 MW during 1000 s to the plasma, in the frequency range 46-65 MHz. Finally an Electron Cyclotron Resonance Heating (ECRH)/Current Drive (ECCD) system has been commissioned in WEST [3]. At frequency 105 GHz, it will supply 1 MW in 2025, and up to 3 MW in 2026. As such, RF power input in WEST plasmas results in dominant electron heating, in part as a result of the D(H) minority scheme typically used for Ion Cyclotron Resonance Heating (ICRH) [4], and low torque injection. This coincides with expectations for ITER, in which large EC power and high-energy NBI ions induce dominant electron heating with relatively modest momentum input [5].

We report here on recent achievements related to the development of steady-state discharges in WEST. Section 2 is devoted to LH-only discharges, which have been designed with the support of extensive integrated modelling, and culminated in the longest duration discharge performed so far in WEST. In section 3, results related to plasma performance enhancement using RF waves, as well as future plans, are underlined.

2 Long-pulse scenarios based on LH power

Achieving long-duration discharges requires minimizing the loop voltage, V_{loop}. One of the most efficient methods to achieve this is to employ LH power for non inductive current drive (CD), and maximize the bootstrap current fraction. For given plasma conditions and in LH power-only pulses, the drop in loop voltage following the application of LH power, P_{LH}, can be approximated as

$$-\frac{\Delta V}{V_\Omega} \equiv \frac{V_\Omega - V_{LHCD}}{V_\Omega} = f_{bs} + \eta_{LH}\frac{P_{LH}}{\bar{n}_l R I_p}, \qquad (1)$$

with V_Ω (resp. V_{LHCD}) the loop voltage prior to (resp. after) the LH power application. f_{bs} is the bootstrap current fraction. $\bar{n}_l$ is the line-averaged plasma density, R the major radius and I_p the total plasma current. η_{LH} is the LHCD efficiency, which depends on various parameters, but was found in several devices to be adequately fitted by a function proportional to $\tau_E^{0.4}$, with τ_E the energy confinement time (see Ref. [6] and references therein). As

*Corresponding author: remi.dumont@cea.fr
**see author list at http://west.cea.fr/WESTteam

a result, the fraction of plasma current supplied by LH waves, I_{LH}/I_p, is proportional to $\tau_E^{0.4} P_{LH}/(\bar{n}_l R I_p)$, showing that non-inductive operation is typically achieved by increasing (resp. decreasing) P_{LH} (resp. $\bar{n}_l$ and/or I_p), while ensuring good confinement. In Fig. 1 is plotted the voltage drop measured at the LH power application in various pulses performed during WEST campaigns C7 to C10 (2023-2025) in the framework of the developments relevant to Long Pulse Operation (LPO). All discharges presented in this manuscript have been performed at nominal magnetic field, i.e. on-axis $B_0 \sim 3.7$ T.

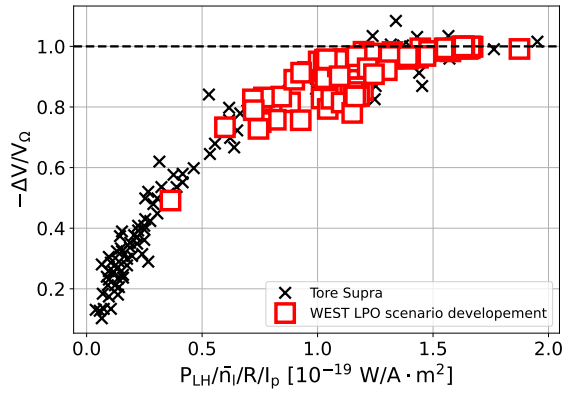

Figure 1. Loop voltage drop (see Eq. 1) in the presence of LH power in Tore Supra (black crosses) and in WEST during the LPO scenario development effort conducted in campaigns C7 to C10 (red squares). The horizontal dashed line represents fully non-inductive operation.

It appears that globally, the results are comparable to what was measured in Tore Supra, a device equipped with a carbon wall. This is consistent with the fact that extensive Fokker-Planck calculations performed with the LUKE code predict that tungsten has a negligible influence on the LHCD efficiency [7]. The relative dispersion of the V_{loop} measurements is attributed to the different range of parameters tested, which results in a finite range of values for τ_E, and thus for η_{LH} and $\Delta V/V_\Omega$.

Operational constraints place restrictions on the available parameter range. In the presence of substantial LHCD power, a fraction of the LH wave-driven energetic electrons can be trapped in the magnetic ripple, and drift upwards. In the fully actively-cooled WEST environment, cooling pipes installed on the upper part of the vacuum vessel can overheat as a result [8]. Measurements of the surface temperature of these elements, T_{pipe}, by the infrared (IR) surveillance system are available in real-time. A thorough study of material fatigue of these elements, as well as calorimetry and IR measurements, have resulted in the definition of a maximum acceptable temperature of 365 °C, which limits the parameter range available for non inductive operation. In Fig. 2, the loop voltage obtained is plotted versus the normalized LH power, $P_{LH}/(\bar{n}_l R I_p)$, for a set of LPO discharges performed during the 2023-2025 campaigns, with the pipe temperature shown in color scale. It confirms the inverse dependence of V_{loop} on this

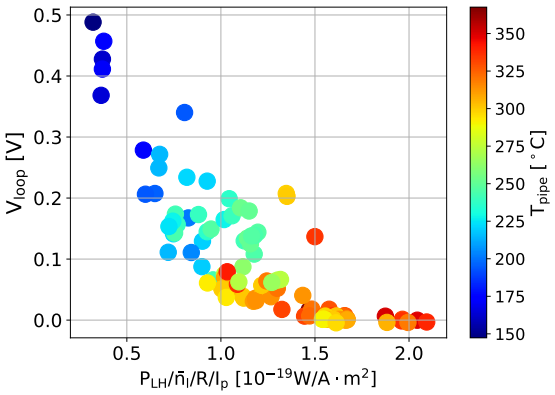

Figure 2. Average value of the loop voltage versus normalized LH power. The color scale shows the corresponding upper pipe temperature as measured by the IR surveillance system.

quantity to lowest order. It also clearly shows that discharges approaching fully non-inductive conditions, i.e. $V_{loop} \sim 0$ V, tend to be accompanied with large values of T_{pipe}.

LH power deposition/current is to a large extent determined by the main plasma parameters. A possible actuator is the toroidal spectrum (see, e.g., Ref. [9]). In order to simultaneously maximize the LHCD efficiency and minimize the upper pipe temperature, several toroidal spectra for each antenna have been tested. In these pulses, the plasma current is feedback-controlled by P_{LH}. The time traces of five of these pulses, each characterized by a central value of $n_\parallel$ averaged over the two launchers according to their respective contribution to the total LH power, and denoted $\langle n_{\parallel,0} \rangle$, are shown in Fig. 3.

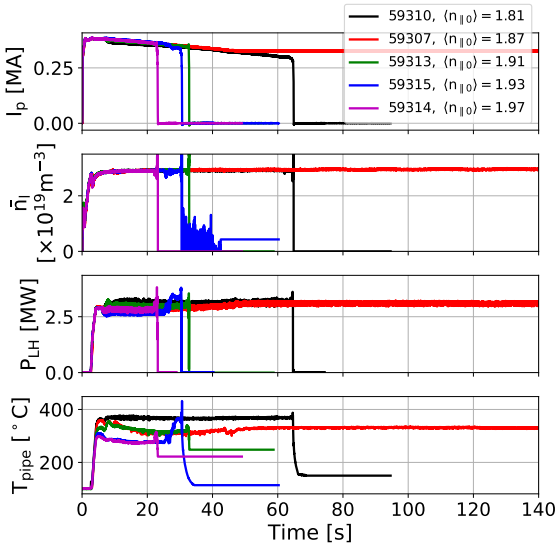

Figure 3. Time traces of five pulses using different combined toroidal spectra. From top to bottom: plasma current, line-averaged density, LH power, pipe temperature.

All these pulses are performed using the same pre-programmed plasma current ramp down, in order to progressively approach non-inductive conditions. It turns out that four out of five are terminated by MHD-induced disruptions, which typically occur when V_{loop} reaches low values [10]. On the other hand, pulse #59310 ($\langle n_{\parallel,0} \rangle$ = 1.81) is characterized by an excessive pipe temperature entailing a reduction of the LH power, which is unable to fulfill the I_p request. Only pulse #59307 ($\langle n_{\parallel,0} \rangle$ = 1.87) reaches 260 s. This confirms the strong influence of the toroidal spectrum, especially since hard X-ray measurements display profiles that are very similar in shape for these discharges.

These results are further summarized in Fig. 4, showing T_{pipe}, the central electron temperature, T_{e0}, and the normalized LH power necessary to sustain the plasma current requested, versus $\langle n_{\parallel,0} \rangle$. All quantities are averaged over time interval t=10-20 s for each pulse.

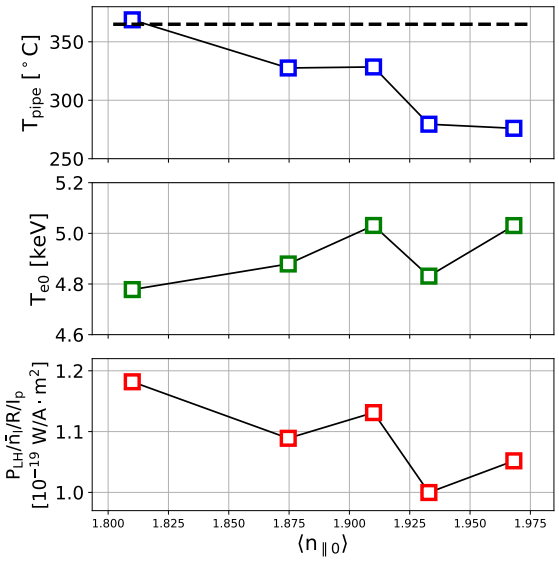

Figure 4. Influence of the central value of the LH parallel refraction index spectrum on (top) the upper pipe temperature, (center) the central electron temperature, and (bottom) the normalized LH power required to sustain the plasma current. All quantities are averaged in time interval t=10-20 s.

It appears that T_{pipe} decreases with $\langle n_{\parallel,0} \rangle$, consistently with LHCD physics and ripple losses dependence, which tend to be lower at larger values of $n_{\parallel}$ [11]. On the other hand, the fact that the LH power decreases is in contradiction with elementary current drive theory, which predicts $\eta_{LH} \propto 1/n_{\parallel}^2$, all other parameters kept constant [12]. This is the result of the considerable influence of the LH current/power deposition profile in these discharges, which determines the dominant heat source as well as the transport properties. The conjunction of the operational constraints, such as described previously, and non-linear effects affecting the plasma discharge as a whole, make it necessary to resort to sophisticated integrated modelling to analyze the results obtained, as well as to design valid non-inductive scenarios with adequate plasma performance [6].

Using this predict-first methodology, during the last WEST campaigns, several duration/energy records have been attained. The culmination of this effort is pulse #61299, lasting 1337 s with an energy injected/extracted of 2.61 GJ. The corresponding main time traces are shown in Fig: 5.

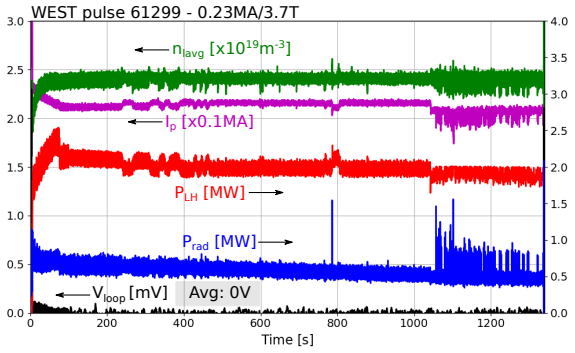

Figure 5. Time traces of fully non inductive WEST pulse #61299. From top to bottom: central line-averaged density, plasma current, LHCD power, radiated power (total), loop voltage.

This pulse has a plasma current $I_p \sim 0.23$ MA, and relies on LH power exclusively. As mentioned previously, I_p is feedback-controlled by P_{LH}, whereas V_{loop} is controlled by the voltage applied to the central solenoid coils. In this discharge, the request is strictly $V_{loop} = 0$ V, which means that the plasma current is entirely the sum of LH and bootstrap contributions. The P_{LH} time trace also shows that the LH power adapts to the plasma conditions in real time. In steady-state, $P_{LH} \sim 2$ MW is necessary to drive the current. The plasma performance is characterized by central electron temperature $T_{e0} \sim 2.0$ keV, confinement factor $H_{98,y2} \sim 0.8$, poloidal beta $\beta_p \sim 1.6$ and normalized toroidal beta $\beta_N \sim 0.6$. This relatively modest performance is the result of mild MHD activity (identified as 3/1 and 4/1 modes) present during the whole duration, which is also the reason for the occasional changes of confinement regime observed between 200 and 500 s (it must be pointed out that the larger change occurring at $t \sim 1040$ s results from a LH klystron failure). This particular pulse is characterized by the fact that only the fully active multi-junction LH launcher was used, in order to relax the constraints on the RF heating systems refrigeration appearing for pulses exceeding 750 s. Bespoke system upgrades will allow these limitations to be alleviated in forthcoming campaigns. Interestingly, long pulses performed with a combination of the two LH launchers and a comparable LH power level, exhibit no MHD, and better confinement. As an example, WEST pulse #60738 (duration 560 s), shown in Fig. 6, uses a combination of the two LH launchers and achieves $T_{e0} \sim 3.4$ keV, $H_{98,y2} \sim 1.1$, $\beta_p \sim 2$ and $\beta_N \sim 0.8$, with negligible MHD activity.

Although it differs from the record pulse in that V_{loop} has a finite value (3 mV), it has been established that the MHD activity in pulse #61299 was unlikely to be caused by the fact that this pulse is fully non inductive. This fur-

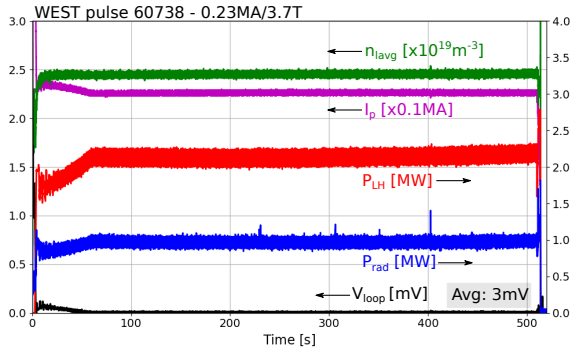

Figure 6. Time traces of WEST pulse #60738, at $V_{loop} = 3$ mV. From top to bottom: central line-averaged density, plasma current, LHCD power, radiated power (total), loop voltage.

ther underlines the sensitivity of the discharge parameters to fine details of the LH current profile. Further data analysis and numerical simulations are ongoing to identify the precise cause for this difference [13].

3 Enhancing long pulse performance with RF power

3.1 ICRH and radiative collapses

In the context of commissioning the ECRH/CD system in WEST and given the fact that modifying the toroidal spectrum of the LH launchers only provides limited effective control, a method to increase the plasma performance is to resort to the ICRF system currently available. In the relatively low density conditions typical of LPO development scenarios, ICRF coupling is known to be challenging, thereby potentially limiting the available power.

The ICRH frequency is typically set around 55.5 MHz, compatible with central power deposition when operating at nominal magnetic field in WEST [4]. The hydrogen minority concentration is around 5% in typical conditions. In Fig. 7 is shown a comparison of two identical shots, #61615 and #61616, except for the fact that 1.2MW of ICRF power is injected in the latter.

The presence of ICRH power makes the LH coupling challenging, as visible from the LH power time trace, and as was already known from previous Tore Supra experience [14]. But another effect of the addition of ICRF power is the fact that the central electron temperature, T_{e0}, drops significantly, and magnetic reconnection events occur before the discharge ends as a result of excessive MHD. This phenomenon has been explained as the result of a radiative collapse, appearing either when density increases [15], and/or when the application of ICRH power results in tungsten accumulation in some cases [16]. As shown in the bottom panel of Fig. 7, the radiated power fraction, f_{rad}, inside normalized radius $\rho = 0.3$ increases significantly in the presence of ICRH. As a result, T_{e0} decreases and the LH power deposition tends to shift outwards [15]. It has been established that the application of ICRF power induces a poloidal asymmetry of the electrostatic potential and a finite toroidal plasma rotation, promoting tungsten accumulation [16]. On the other hand, the central ICRF power in these conditions should result in significant electron heating through collisional relaxation of the driven energetic ions [4].

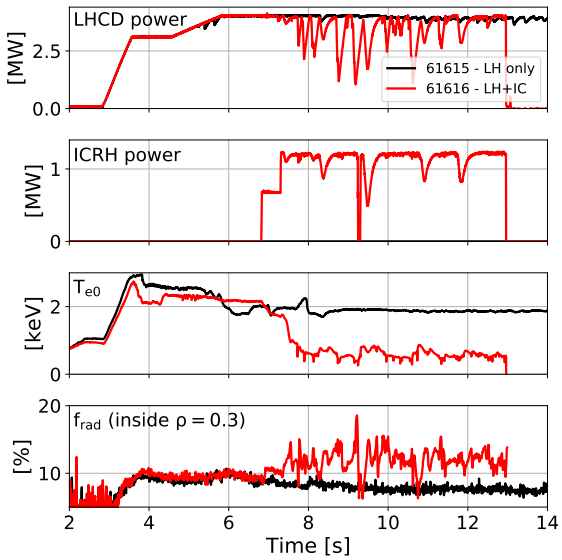

Figure 7. A comparison of WEST pulses 61615 (black) and 61616 (red), differing in that the latter features 1.2MW ICRH power. From top to bottom: LHCD power, ICRH power, central electron temperature and fraction of radiated power (in %), inside normalized radius $\rho = 0.3$.

In order to investigate this issue, detailed RF simulations have been performed, using the EVE/AQL full wave/Fokker-Planck code [17]. This study was conducted in the conditions of ICRH-only pulse #55605, for which 1) a detailed study of the power radiation by impurities has been conducted, and 2) the level of power lost in the magnetic ripple can be estimated from IR images of the baffle, which was not actively cooled at the time this discharge was performed [18]. Although the parameters differ from the collapsing pulse shown in Fig. 7, it is believed that the mechanism leading to the collapse is similar. Time traces of the ICRH power applied and the central electron temperature are shown in Fig. 8.

In WEST pulse #55605, it has been established that the radiated power inside normalized radius $\rho = 0.3$ is of the order of $P_{rad}(\rho \leq 0.3) \sim 0.5$ MW at t=5.6 s, when the collapse starts.

3.2 Finite orbit width effects

Self-consistent RF simulations have been performed, using the experimental parameters measured at this time. The minority concentration is assumed to be $n_H/n_e = 5\%$, in agreement with spectroscopy measurements. The ICRF power is 3.8 MW, the frequency is $P_{ICRH} = 55.5$ MHz and the toroidal spectrum corresponds to dipole phasing, $(0, \pi)$. For these simulations, ten toroidal modes are retained, ranging from -47 to +47. Fig. 9 shows the results obtained using EVE/AQL, in which it is assumed by default that ion orbits are infinitely thin [17].

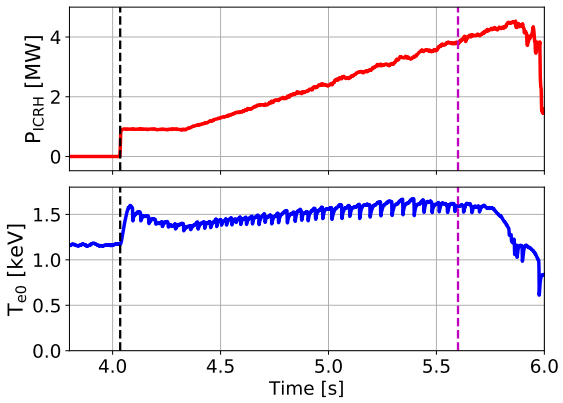

Figure 8. WEST pulse #55605. (Top panel) ICRH power; (Bottom panel) Central electron temperature. The two dashed line show the RF application time (left) and the EVE/AQL simulation time (right).

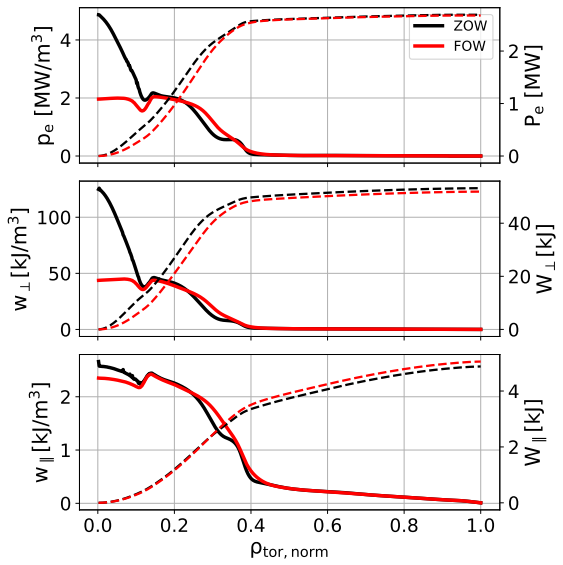

Figure 9. Comparison between EVE solution without (black) and with (red) FOW effects, using the reduced model described in the main text. From top to bottom: power to electrons, minority hydrogen perpendicular energy, minority hydrogen parallel energy. Left axis: power/energy density (solid lines); Right axis: cumulative power/energy between axis and current normalized radius (dashed lines).

One of the most important outcomes of these simulations is the large power level transferred from minority ions to electrons by collisional relaxation (top panel of Fig. 9). At 5% concentration, it is predicted that the power density source on the magnetic axis exceeds 4.8 MW/m^3, and the heating source inside $\rho = 0.3$ is of the order $P_e(\rho \leq 0.3) \sim 2.15$ MW. This power level is well in excess of the 0.5 MW radiated power mentioned previously, i.e. should prevent the radiative collapse from occurring.

As shown in Fig. 9, in these simulations, the perpendicular energy appears to be quite peaked on the magnetic axis, which is the reason for the large power source on electrons. One potential caveat is the Zero Orbit Width (ZOW) limit assumed by default in AQL. In a medium size tokamak such as WEST, it is clear that trapped energetic ions are characterized by banana/potato orbits with typical widths representing a significant fraction of the plasma minor radius. In order to take this effect into account, a bespoke reduced model for Finite Orbit Width (FOW) effects has been implemented in AQL.

At each point $(v_\parallel, v_\perp, r)$ in phase space, with $v_\parallel$ (resp. $v_\perp$) the parallel (resp. perpendicular) velocity, the trapped orbit (potato or banana, whichever applicable) width, δ_{tr}, is computed according to

$$\delta_{tr}(v_\parallel, v_\perp, r) \equiv \begin{cases} \delta_b(v_\parallel, v_\perp, r) & \text{if } \delta_b \leq r, \\ \delta_p(v_\parallel, v_\perp, r) & \text{otherwise} \end{cases} \quad (2)$$

with δ_b (resp. δ_p) the banana (resp. potato) width [19].

This width is then averaged over velocity-space as

$$\delta_{FOW}(r) \equiv \frac{\int_{tr} d^3\mathbf{v} f_H(v_\parallel, v_\perp, r)\delta_{tr}(v_\parallel, v_\perp, r)}{\int_{tr} d^3\mathbf{v} f_H(v_\parallel, v_\perp, r)}, \quad (3)$$

with f_H the computed hydrogen distribution function, and where the integral is carried over the trapped part of velocity space to obtain a radial profile. This quantity is then used to enlarge the power density profile in the EVE/AQL calculation, using a convolution of the ZOW profile with a Gaussian function of typical width δ_{FOW}. The FOW model is applied throughout all the EVE/AQL iterative process. A first EVE calculation is performed, yielding a ZOW power deposition profile. This profile is used by AQL to compute a first estimate of the minority distribution function. From this distribution, the averaged orbit width, δ_{FOW}, is obtained (Eq. 3). EVE is run a second time with the previous minority distribution parameters as input, and an updated power deposition profile is obtained, still in the ZOW limit. Before the second AQL run, the convolution procedure is applied to the power deposition from EVE, using the width computed previously to obtain an enlarged (FOW) deposition profile. From this point on, every iteration is performed with a FOW deposition profile based on δ_{FOW} from the previous iteration. Typically, for the WEST minority heating simulations presented in this article, the profiles/distributions obtained are found not to evolve significantly after 5-6 iterations, similarly to ZOW EVE/AQL calculations published previously [17].

The final result of this procedure is a new profile, labeled FOW, also shown in Fig. 9. It appears that the perpendicular energy, and the power transferred from minorities to electrons, is significantly reduced in the central region of the plasma (where the trapped particle width is the largest). The parallel energy, on the other hand, is only affected in a limited, yet non-zero, fashion, as the reduced anisotropy results in a slightly modified balance between pitch-angle scattering and wave-induced diffusion [20].

It should be pointed out that, although such a reduced model does not aim to replace more advanced calculations (Monte Carlo or others), the resulting power deposition profile appears to be more realistic than the one obtained in the ZOW approximation. To illustrate this point, a break-in slope (BIS) analysis (see, e.g., Ref. [21]) based on electron temperature measurement by the Electron Cyclotron

Emission (ECE) radiometer around the ICRH switch-on time (t=4.04 s), as been performed to evaluate the power source on electrons. One caveat, in this pulse, is that for operational reasons, the ICRF power is not increased directly to its final value (3.8 MW) but rather to a smaller level (0.9 MW in this case), and then ramped up progressively (see. Fig. 8). An accurate BIS estimate, on the other hand, requires an abrupt switch-on. This means that the BIS analysis can only be reliably performed at the 0.9 MW power level, and compared to numerical simulations using the same power, for which FOW effects clearly play a less important role than at 3.8 MW. The corresponding EVE/AQL calculations have been performed: one in the ZOW limit and one in which the FOW model is used, both at total ICRH power 0.9 MW. The total electron power source, resulting from collisional relaxation of minority ions and direct Electron Landau damping, although the latter effectively contributes very little, is shown in Fig. 10.

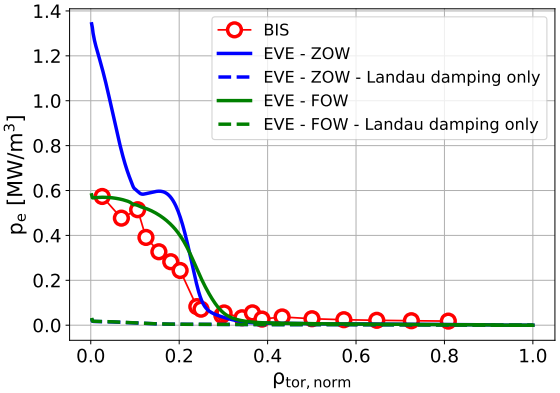

Figure 10. A comparison of power source on electrons from BIS analysis (red circles), and EVE/AQL calculation in the ZOW limit (blue) and in the FOW limit (green). The contribution of Electron Landau damping in both case is also shown as dashed lines.

In this situation, the FOW result appears to be more consistent with the experimental evaluation than the ZOW simulation, adding some credibility to the fact that FOW effects probably play an important role in WEST, and should be included to explain measurements.

Despite this refinement, it is found that the power density near the magnetic axis is $p_e(0) \sim 2$ MW/m^3 and the cumulative power to electrons inside $\rho = 0.3$ is $P_e(\rho \leq 0.3) \sim 2.02$ MW. Both quantities are still well in excess of the estimated radiated power inside $\rho = 0.3$, $P_{rad}(\rho \leq 0.3) \sim 0.5$ MW, and this calculation thus still does not suffice to justify the radiative collapse observed.

3.3 Ripple-induced losses of energetic ions

Another potential source of power source deficit on electrons is the loss of energetic ions. Owing to its finite number of toroidal coils, WEST has a magnetic ripple level on the outboard side of the plasma ($R \sim 2.93$ m) up to 2.3%. This effect is a well-known potential source of ICRF-driven ion losses. The lost energetic ions drift downwards, impinging plasma facing components installed in the lower part of WEST, most notably the baffle [18]. A consequence of this phenomenon is a deficit in plasma heating by collisional relaxation of energetic ions. In this particular pulse, it is estimated that 20% of the ICRF power is lost [16]. The impact of this lost power on the amount of electron heating has been investigated using EVE/AQL. In order to account for this effect in a simplified fashion, it is assumed in AQL that all ions above a certain energy, E_{loss}, are lost. For each simulation, the corresponding value of lost power, P_{loss}, is obtained, and f_{loss} is defined as the ratio of this lost power to the total ICRF power. Figure 11 shows E_{loss} vs f_{loss} (top panel).

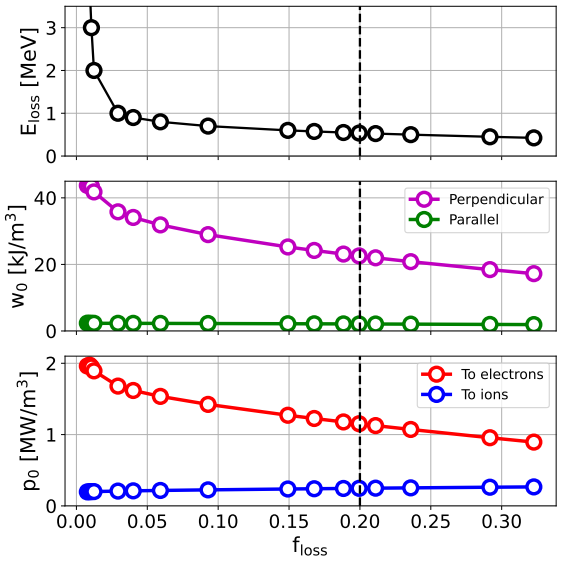

Figure 11. EVE calculation of the impact of losses above E_{loss} on the central perpendicular/parallel energy density (middle panel) and the central power density transferred to electrons/ions (bottom panel). The x-axis shows the corresponding ICRF power loss, which is estimated to be 20% in this pulse (dashed line).

According to this simplified model, $f_{loss} = 20\%$ is obtained when all ions above $E_{loss} \sim 540$ keV are assumed lost in the ripple, therefore not contributing to plasma heating. The central panel of Fig 11 shows that this has the largest impact on the central perpendicular energy, which results from the large perpendicular temperature typical of ICRF-driven energetic ions. As shown on the bottom panel of the same figure, the impact on the electron heating is considerable: 20% of power losses translates in reduction of the power source on electrons by a factor 2. It is worthwhile noting that the fraction of power on ions increases slightly as E_{loss} decreases, which is caused by the fact that these simulations are self-consistent: a modification of the minority ion distribution caused by losses can result in a modification of the overall power split between species.

In Fig. 12 is summarized the results obtained in terms of electron power source profile: ZOW, FOW, FOW with 20% ripple losses.

It can be noted that the profile total power on electrons inside $\rho = 0.3$ is now of the order of 0.5 MW, which is comparable to the limit for radiative collapse. It should be

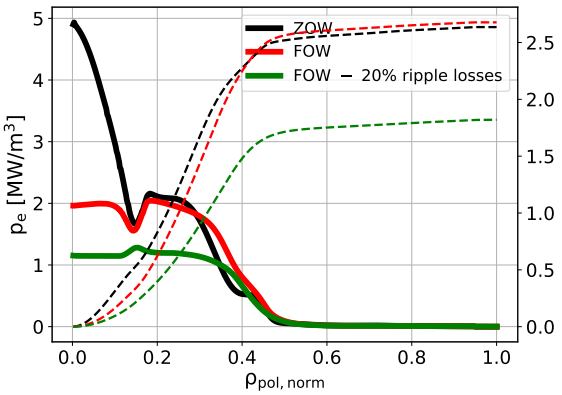

Figure 12. Comparison of power density on electrons when only ZOW effects are included (black), FOW effects are included (red) and FOW effects with 20% ripple losses are taken into account (green). Left axis: power density (solid lines); Right axis: cumulative power between axis and current normalized radius (dashed lines).

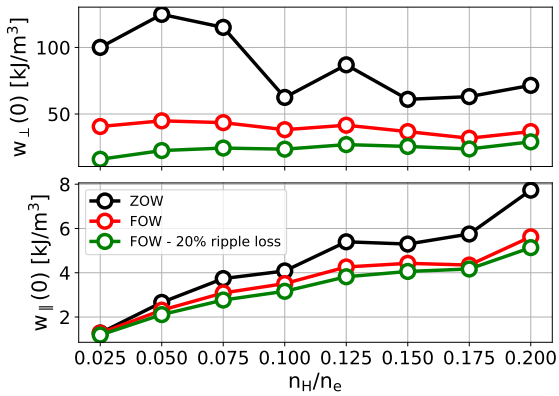

Figure 13. Effect of the minority concentration n_H/n_e on the perpendicular (top); parallel (bottom) energetic ion energy density on the magnetic axis in the ZOW (black), FOW (red) and FOW including 20% power loss (green) limit.

recalled, however, that the application of ICRF also contributes to tungsten accumulation from the poloidal asymmetry of the potential, and increased plasma toroidal rotation, so that it can explain the fact that radiative collapses are observed even in the presence of an electron power source comparable in magnitude in the plasma center.

3.4 Minority concentration scans

A rather straightforward possibility to reduce the level of ripple losses is to increase the minority concentration [11]. Indeed, to lowest order, the amount of energy available per minority ion when increasing n_H/n_e is reduced in proportion [20]. This possibility was investigated by using EVE/AQL, varying the minority concentration between 2.5 and 20%, whereas all other parameters are assumed constant. The increase in hydrogen concentration is compensated by decreasing the deuterium concentration accordingly.

Fig. 13 shows the variation of $w_\perp(0)$ (resp. $w_\parallel(0)$), the central perpendicular (resp. parallel) energy density in the three limits discussed in the context of Fig. 12.

In the ZOW limit, $w_\perp(0)$ is found to globally decrease as n_H/n_e increases, in agreement with Ref. [20], although it is worth noting that this decrease is not strictly monotonic, as changes in the wave propagation/damping usually make the picture more complex. Interestingly, in the FOW limit including losses, an opposite trend is observed: the perpendicular temperature increases slightly, as energetic ion losses tend to decrease and eventually result in overall enhanced electron heating. $w_\parallel(0)$, on the other hand, increases monotonically in the three cases as a result of pitch-angle scattering. The consequences in terms of central electron / bulk ion heating are shown in Fig. 14.

The results obtained stem directly from the previous observations related to Fig. 13: unsurprisingly, central electron heating follows the same trend as $w_\perp(0)$, whereas central ion heating increases continuously in the three

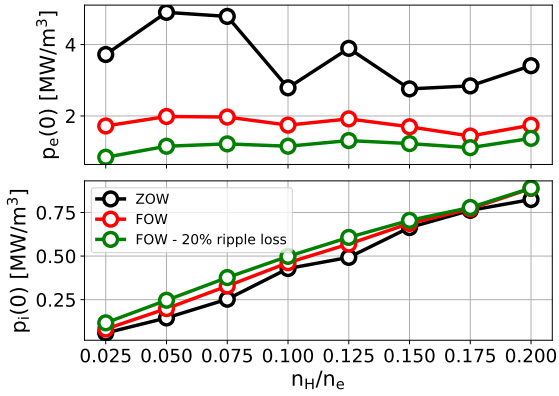

Figure 14. Effect of the minority concentration n_H/n_e on the electron (top); ion (bottom) power density received from minority ions on the magnetic axis in the ZOW (black), FOW (red) and FOW including 20% power loss (green) limit.

cases since increasing n_H/n_e tends to increase the relative contribution of the low/medium energy part of the minority ion tail to collisional power transfers.

Although increasing the minority concentration therefore appears as a valid option to increase the power source on electrons in the presence of energetic ion losses, it is also well known that the global wave per-pass damping rate decreases as n_H/n_e increases, favoring impurity-related issues, potentially problematic in metallic environments (see, e.g., Refs. [22, 23]). Although the single pass (SP) damping rate does not constitute an unequivocal assessment of the quality of a given ICRF scenario, especially in metallic environments [24], it usually constitutes a good indicator of potential difficulties when it reaches low values. In order to evaluate this quantity in WEST, the 1D all-orders full wave code METS [25, 26] has been employed, using the parameters of pulse #55605 at various concentrations. The result is shown in Fig. 15.

It is found that the wave damping is largely dominated by the hydrogen minority ions in all cases. Elec-

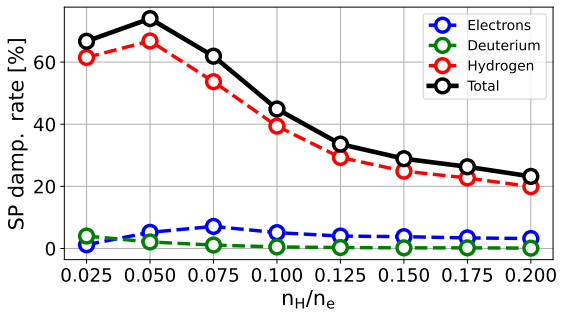

Figure 15. Estimate of the single pass damping rate when n_H/n_e is varied: electrons (dashed blue), deuterium (dashed green), hydrogen (dashed red); total (solid black).

trons and deuterium absorb only a small amount of the injected power. The total single pass damping rate is maximum at $n_H/n_e \sim 5\%$, which is in line with previous findings [23, 27]. It drops below 30% for $n_H/n_e \sim 15\%$. Although the development of the energetic ion tail can potentially result in an increase of this damping rate [26], the phase during which this tails builds up could be characterized by operational difficulties.

Another possibility to strongly reduce the amount of ripple losses is to operate at larger densities, as the power lost scales as $\bar{n}_l^{\beta_2}$ with $\beta_2 = -2.16 \pm 0.76$. This is also favorable for a reliable use of ICRH power in these discharges [18], which has been shown in the past to be beneficial in terms of MHD stability in non-inductive pulses [28]. However, operating at larger densities also requires a larger power level available for current drive. One appealing possibility is to use the ECRH/ECCD system recently installed in WEST [3]. In 2025, 1 MW of EC power is available for plasma heating/current drive with a total power installed eventually planned to reach 3 MW in 2026. This is expected to significantly enlarge the parameter space and increase the performance of non-inductive discharges based on LHCD, as reported in recent experiments (see, e.g., Refs. [29, 30]). As observed in the numerical simulations in Ref. [6], the application of central ECCD is expected to be instrumental in controlling the safety factor profile reversal inherent to LHCD plasmas as well as improving the overall current drive efficiency, thus allowing non-inductive operation at larger densities. The LH-EC synergy, not included in Ref. [6], is also expected to further contribute to this enhancement [31]. As discussed in Ref. [16], by supplying an additional localized electron source in the plasma core, EC power should be an efficient method to counterbalance radiative collapses such as shown in this work. In addition, the prospect of a future Travelling Wave Array (TWA) antenna installed in WEST will provide additional flexibility in the heating methods available for long pulse, high-performance scenario development [32]. It is expected that this unique combination of LH, IC and EC power will allow WEST to further investigate issues relevant to the operation of future fusion devices with full metal environments.

4 Conclusions

Significant progress has been achieved in next-step relevant developments in the WEST tokamak, which relies exclusively on RF power for auxiliary plasma heating/current drive. Among recent accomplishments, long duration pulses have been achieved, based on LHCD power. In LHCD-only pulses, the toroidal phasing offers only limited flexibility, as LHCD-induced reversed safety factor profiles are prone to the triggering of instabilities. This experimental result confirms the fact that numerical simulations including a self-consistent description of current diffusion, heat sources, and heat and particle transport, are required to model these non-inductive pulses. With the support of predict-first integrated modelling, long duration discharges up to 22 min with 2.61 GJ energy injected/extracted have been performed. ICRF waves have been employed to increase the plasma performance in these low/zero loop voltage, low density, discharges. However, in the absence of any particular wall conditioning procedure, radiative collapses are often observed, resulting from an excessive core radiation by tungsten, only partly compensated by electron heating from energetic ICRF-driven minority ions. The EVE/AQL code has been employed to investigate this issue in detail. Using a reduced model, it was shown that FOW effects needed to be included to describe the ICRF-induced electron heating source in medium size devices such as WEST. Furthermore, discharges in which ion ripple losses were deduced from IR measurements have been used to estimate an energy limit, above which energetic ions are assumed lost. Adding this effect to simulations has confirmed that the combination of FOW effects and ripple losses could explain the electron heating deficit, and radiative collapses observed. Finally, the influence of increasing the minority concentration has been investigated. It has been shown that whereas $n_H/n_e \sim 5$ % was optimal in ZOW conditions and no losses, increasing this value could allow core electron heating to be optimized when FOW effects and ripple losses are included. Single-pass damping rate estimates performed with the METS code show that increasing n_H/n_e up to 10% allows a single-pass damping rate above 40% to be maintained.

In general, higher density operation is desirable to help coupling ICRF waves, decrease ripple losses (electron and ion) and improve plasma performance. Upgrades of the WEST RF capabilities are expected to contribute to core electron heating in this context: a TWA antenna operating in the IC range of frequencies, and an ECRH/ECCD system. In addition to various other technical device improvements, these upgrades are expected to facilitate further developments of RF-based high performance scenarios in WEST in upcoming campaigns.

5 Acknowledgments

This project was provided with computer and storage resources by GENCI at TGCC thanks to the grant 2024-A0170500198 on the ROME partition of the Joliot Curie computer.

References

[1] J. Bucalossi, A. Ekedahl, the WEST Team, J. Achard, K. Afonin, O. Agullo, T. Alarcon, L. Allegretti, F. Almuhisen, H. Ancher et al., WEST full tungsten operation with an ITER grade divertor, Nuclear Fusion **64**, 112022 (2024). https://doi.org/10.1088/1741-4326/ad64e5

[2] X. Litaudon, H.S. Bosch, T. Morisaki, M. Barbarino, A. Bock, E. Belonohy, S. Brezinsek, J. Bucalossi, S. Coda, R. Daniel et al., Long plasma duration operation analyses with an international multi-machine (tokamaks and stellarators) database, Nuclear Fusion **64**, 015001 (2023). https://doi.org/10.1088/1741-4326/ad0606

[3] L. Delpech, S. Alberti, K. Avramidis, A. Ayreault, T. Batal, J.M. Bernard, F. Bouquey, I. Chelis, F. Clairet, E. Corbel et al., A new 3MW ECRH system at 105GHz for WEST, Fusion Engineering and Design **186**, 113360 (2023). https://doi.org/10.1016/j.fusengdes.2022.113360

[4] C. Bourdelle, J. Artaud, V. Basiuk, M. Bécoulet, S. Brémond, J. Bucalossi, H. Bufferand, G. Ciraolo, L. Colas, Y. Corre et al., WEST physics basis, Nuclear Fusion **55**, 063017 (2015). https://doi.org/10.1088/0029-5515/55/6/063017

[5] R. Pitts, A. Loarte, T. Wauters, M. Dubrov, Y. Gribov, F. Köchl, A. Pshenov, Y. Zhang, J. Artola, X. Bonnin et al., Plasma-wall interaction impact of the ITER re-baseline, Nuclear Materials and Energy **42**, 101854 (2025). https://doi.org/10.1016/j.nme.2024.101854

[6] T. Fonghetti, P. Manas, R. Dumont, J.F. Artaud, C. Bourdelle, F. Casson, N. Cummings, L. Delgado-Aparicio, P. Maget, J. Morales et al., WEST L-mode record long pulses guided by predictions using integrated modeling, Nuclear Fusion **65**, 056018 (2025). https://doi.org/10.1088/1741-4326/adc7c7

[7] Y. Peysson, D. Mazon, A. Jardin, K. Król, J. Bielecki, D. Dworak, M. Scholz, O. Embréus, L. Hesslow, T. Fülop et al., Effect of partially ionized high-Z atoms on fast electron dynamics in tokamak plasmas, 28th IAEA Fusion Energy Conference, IAEA FEC 2020 (2021).

[8] J. Morales, T. Fonghetti, T. Barbui, P. Manas, C. Bourdelle, P. Maget, R. Dumont, S. Mazzi, J.F. Artaud, A. Ekedahl et al., Operational space for lower hybrid heating scenarios in the full tungsten environment of WEST, Nuclear Fusion **65**, 106003 (2025). https://doi.org/10.1088/1741-4326/adf7be

[9] F. Imbeaux, M. Lennholm, A. Ekedahl, P. Pastor, T. Aniel, S. Brémond, J. Decker, P. Devynck, R. Dumont, G. Giruzzi et al., Real-time control of the safety factor profile diagnosed by magneto-hydrodynamic activity on the Tore Supra tokamak, Nuclear Fusion **51**, 073033 (2011). https://doi.org/10.1088/0029-5515/51/7/073033

[10] P. Maget, F. Imbeaux, G. Huysmans, F. Clairet, P. Moreau, J.L. Segui, L. Vermare, M. Ottaviani, M. Goniche, MHD stability of fully non-inductive discharges in Tore Supra, Nuclear Fusion **45**, 69 (2005). https://doi.org/10.1088/0029-5515/45/2/001

[11] V. Basiuk, Y. Peysson, M. Lipa, G. Martin, M. Chantant, D. Guilhem, F. Imbeaux, R. Mitteau, F. Surle, Studies of suprathermal electron loss in the magnetic ripple of Tore Supra, Nuclear Fusion **41**, 477 (2001). https://doi.org/10.1088/0029-5515/41/5/301

[12] N.J. Fisch, Theory of current drive in plasmas, Rev. Mod. Phys. **59**, 175 (1987). https://doi.org/10.1103/RevModPhys.59.175

[13] R.J. Dumont, T. Fonghetti, P. Maget, P. Manas, J.F. Artaud, T. Barbui, C. Bourdelle, L. Colas, G. Ciraolo, Y. Corre et al., WEST long-pulse achievements in support of next-step fusion devices, Nuclear Fusion (Manuscript in preparation, 2026).

[14] A. Ekedahl, V. Basiuk, J. Bucalossi, L. Colas, Y. Corre, R. Dumont, L. Eriksson, M. Goniche, J.P. Gunn, F. Kazarian et al., RF coupling and antenna heat load control for combined LHCD and ICRH in Tore Supra, AIP Conference Proceedings **933**, 237 (2007). https://doi.org/10.1063/1.2800483

[15] V. Ostuni, J. Morales, J.F. Artaud, C. Bourdelle, P. Manas, N. Fedorczak, R. Dumont, M. Goniche, P. Maget, Y. Peysson et al., Core radiative collapse characterisation and integrated modelling in WEST plasmas, Nuclear Fusion **62**, 106034 (2022). https://doi.org/10.1088/1741-4326/ac8cd6

[16] P. Maget, P. Manas, R. Dumont, C. Angioni, J.F. Artaud, C. Bourdelle, F.J. Casson, L. Colas, P. Devynck, D. Fajardo et al., Tungsten accumulation during ion cyclotron resonance heating operation on WEST, Plasma Physics and Controlled Fusion **65**, 125009 (2023). https://doi.org/10.1088/1361-6587/ad09fd

[17] R. Dumont, D. Zarzoso, Heating and current drive by ion cyclotron waves in the activated phase of ITER, Nuclear Fusion **53**, 013002 (2012). https://doi.org/10.1088/0029-5515/53/1/013002

[18] D. Moiraf, J. Morales, L. Colas, N. Fedorczak, J. Gaspar, R. Dumont, the WEST Team, Optimization of the operational domain for ICRH scenarios in WEST from statistical analysis, Nuclear Fusion **63**, 086010 (2023). https://doi.org/10.1088/1741-4326/acdca4

[19] L.G. Eriksson, F. Porcelli, Dynamics of energetic ion orbits in magnetically confined plasmas, Plasma Physics and Controlled Fusion **43**, R145 (2001). https://doi.org/10.1088/0741-3335/43/4/201

[20] T. Stix, Fast-wave heating of a two-component plasma, Nuclear Fusion **15**, 737 (1975). https://doi.org/10.1088/0029-5515/15/5/003

[21] E.A. Lerche, D. Van Eester, JET EFDA contributors, Improved break-in-slope analysis of the plasma energy response in tokamaks, Plasma Physics and Controlled Fusion **50**, 035003 (2008). https://doi.org/10.1088/0741-3335/50/3/035003

[22] S. Wukitch, B. LaBombard, Y. Lin, B. Lipschultz, E. Marmar, M. Reinke, D. Whyte, ICRF specific im-

purity sources and plasma sheaths in Alcator C-Mod, Journal of Nuclear Materials **390-391**, 951 (2009). https://doi.org/10.1016/j.jnucmat.2009.01.245

[23] E. Lerche, M. Goniche, P. Jacquet, D. Van Eester, V. Bobkov, L. Colas, C. Giroud, I. Monakhov, F. Casson, F. Rimini et al., Optimization of ICRH for core impurity control in JET-ILW, Nuclear Fusion **56**, 036022 (2016). https://doi.org/10.1088/0029-5515/56/3/036022

[24] D. Van Eester, E. Lerche, P. Jacquet, V. Bobkov, A. Czarnecka, J.W. Coenen, L. Colas, K. Crombé, M. Graham, S. Jachmich et al., Effect of the minority concentration on ion cyclotron resonance heating in presence of the ITER-like wall in JET, AIP Conference Proceedings **1580**, 223 (2014). https://doi.org/10.1063/1.4864528

[25] D.N. Smithe, C.K. Phillips, J.C. Hosea, R.P. Majeski, J.R. Wilson, Investigation of rf absorption by fast ions and high temperature plasmas using the "METS95" wave analysis tool, AIP Conference Proceedings **403**, 367 (1997). https://doi.org/10.1063/1.53349

[26] R.J. Dumont, C.K. Phillips, D.N. Smithe, Effects of non-Maxwellian species on ion cyclotron waves propagation and absorption in magnetically confined plasmas, Physics of Plasmas **12**, 042508 (2005). https://doi.org/10.1063/1.1881472

[27] M. Goniche, V. Ostuni, C. Bourdelle, P. Maget, J. Artaud, J. Bernard, V. Bobkov, J. Bucalossi, F. Clairet, L. Colas et al., Developing high performance RF heating scenarios on the WEST tokamak, Nuclear Fusion **62**, 126058 (2022). https://doi.org/10.1088/1741-4326/ac9691

[28] R.J. Dumont, M. Goniche, A. Ekedahl, B. Saoutic, J.F. Artaud, V. Basiuk, C. Bourdelle, Y. Corre, J. Decker, D. Elbèze et al., Multi-megawatt, gigajoule plasma operation in Tore Supra, Plasma Physics and Controlled Fusion **56**, 075020 (2014). https://doi.org/10.1088/0741-3335/56/7/075020

[29] H. Du, S. Ding, J. Chen, Y. Wang, H. Lian, G. Xu, X. Zhai, H. Liu, Q. Zang, B. Lyu et al., Analysis of performance degradation in an electron heating dominant H-mode plasma after ECRH termination in EAST, Nuclear Fusion **58**, 066011 (2018). https://doi.org/10.1088/1741-4326/aabaab

[30] M. Li, H. Xu, X. Wang, M. Wang, B. Ding, C. Wu, G. Yan, L. Liu, L. Zhao, Z. Wu et al., Plasma heating by electron cyclotron wave and the temperature effects on lower hybrid current drive on EAST, Nuclear Fusion **63**, 046019 (2023). https://doi.org/10.1088/1741-4326/acbec9

[31] G. Giruzzi, J.F. Artaud, R.J. Dumont, F. Imbeaux, P. Bibet, G. Berger-By, F. Bouquey, J. Clary, C. Darbos, A. Ekedahl et al., Synergy of electron-cyclotron and lower-hybrid current drive in steady-state plasmas, Phys. Rev. Lett. **93**, 255002 (2004). https://doi.org/10.1103/PhysRevLett.93.255002

[32] R. Ragona, F. Durodié, A. Messiaen, J. Ongena, M. Van Schoor, S. Agzaf, T. Batal, J.M. Bernard, X. Courtois, J.M. Delaplanche et al., Status of the WEST travelling wave array antenna design and results from the high power mock-up, Nuclear Fusion **62**, 026046 (2022). https://doi.org/10.1088/1741-4326/ac4467